

Tetranitratopalladate(II) Salts with Tetraalkylammonium Cations: Structural Aspects, Reactivity, and Applicability toward Palladium Deposition for Catalytic Applications

Danila Vasilchenko,* Polina Topchiyan, Semen Berdyugin, Pavel Plyusnin, Vladimir Shayapov, Iraida Baidina, Vladislav Komarov, Andrey Bukhtiyarov, and Evgeny Gerasimov

Cite This: *Inorg. Chem.* 2021, 60, 2983–2995

Read Online

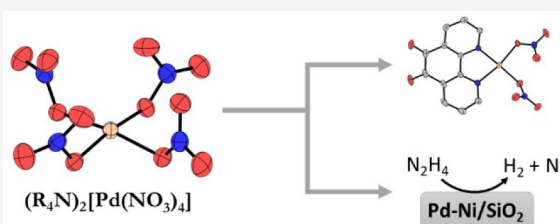
ACCESS |

Metrics & More

Article Recommendations

Supporting Information

ABSTRACT: A series of salts $(R_4N)_2[Pd(NO_3)_4]$ ($R = CH_3, C_2H_5, n-C_3H_7$; 1–3) were synthesized in high yield from a nitric acid solution of palladium. The salts were characterized by a combination of physicochemical methods, and their crystal structures were determined by X-ray diffraction. The conformation of the $[Pd(NO_3)_4]^{2-}$ anion was studied in detail using crystal structure data and density functional theory calculations. A combination of nonhygroscopicity and stability under normal conditions, together with thermolability, high solubility in various solvents, and the lability of nitrate ligands, makes salts 1–3 valuable starting materials for the synthesis of Pd compounds and the preparation of Pd-containing catalysts. In this work, these applications were illustrated by the synthesis of heteroleptic Pd(II) nitrate complexes with N-donor ligands and the preparation of $Pd_{0.1}Ni_{0.9}/SiO_2$ catalysts, which worked well in H_2 generation from hydrazine hydrate. Generally, it was shown that up to several weight percent of Pd can be deposited on various oxide/hydroxide supports using a straightforward chemisorption procedure from acetone solutions of 1–3.



1. INTRODUCTION

Materials prepared by the deposition of palladium on diverse supports are widely used in heterogeneous catalysis, accounting for about 90% of the annual demands of this metal.¹ The most resource-intensive application of such materials is in the automotive emission depollution system,^{2,3} but they are also vital for important industrial processes, such as ethylene glycol synthesis (via dimethyl oxalate)⁴ and the production of purified terephthalic acid.^{5,6} Along with other noble metals, Pd-containing catalysts are of great interest to research directed toward the development of hydrogen energy systems, including fuel cell fabrication,⁷ hydrogen storage,^{8,9} and hydrogen generation.^{10,11}

Among the palladium-containing compounds used for the preparation of supported catalysts, the palladium nitrate $trans-[Pd(NO_3)_2(H_2O)_2]$ (CAS: 32916-07-7) is of great importance.^{12–14} The thermolability of this reagent is a major advantage (decomposition at about 100 °C),¹⁵ resulting in the ready formation of metallic Pd nanoparticles or ionic Pd species on the surface of the support under mild conditions.¹⁶ Furthermore, the substitutional lability of the nitrate ligands in $[Pd(NO_3)_2(H_2O)_2]$ provide a straightforward route to the heteroleptic palladium(II) complexes by the sequential reactions $[Pd(NO_3)_2(H_2O)_2] \rightarrow [Pd(NO_3)_2L^1_2] \rightarrow [PdL^2_2L^1_2]$.¹⁷

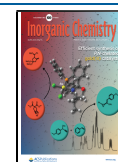
Despite the noted benefits, the hygroscopicity of this palladium nitrate causes difficulties in handling, especially

after prolonged storage. The closely related thermolabile salts $(NO)_2[Pd(NO_3)_4]$ and $Pd(NO_3)_2$ can be prepared by dissolution of Pd in liquid N_2O_5 or fuming HNO_3 ; unfortunately, they are extremely sensitive to moisture.^{18,19} The series of salts $M_2[Pd(NO_3)_4]$ ($M = Na, K, Rb, Cs$) were also synthesized^{20–22} and characterized, but their lack of solubility in organic solvents and the unavoidable residue of MNO_3 salts make them less attractive as starting compounds for catalyst preparation and synthesis.

Recently, we have reported on anionic platinum nitrate complexes, which were isolated as the tetraalkylammonium salts $(R_4N)_2[Pt(NO_3)_6]$ and $(R_4N)_2[Pt_2(OH)_2(NO_3)_8]$ ($R = CH_3, \dots, C_4H_9$).^{23,24} These salts are stable under normal conditions, possess a high solubility in various organic solvents, and decompose at moderate temperatures. Moreover, the chemisorption of platinum onto ceria and titania from acetone solutions of the nitrate complexes was successfully utilized as a method for the preparation of efficient catalysts for CO

Received: October 14, 2020

Published: February 10, 2021



oxidation^{23,25} (Pt/CeO₂) and H₂ photogeneration (Pt/TiO₂).²⁶

In this work, we describe the method of preparation, structure, and properties of the series of salts (R₄N)₂[Pd(NO₃)₄] (R = CH₃, C₂H₅, n-C₃H₇, 1–3). Essentially, these tetranitratopalladate anion containing salts are useful starting compounds due to their stability under normal conditions and nonhygroscopicity, combined with the general lability and thermolability of nitrate complexes. The applicability of salts 1–3 as suitable materials for the synthesis of palladium complexes and the preparation of catalysts were demonstrated by the synthesis of heteroleptic Pd(II) nitrate complexes with N-donor ligands and the preparation of Pd_{0.1}Ni_{0.9}/SiO₂ catalysts, which are effective in hydrazine hydrate decomposition.

2. EXPERIMENTAL SECTION

2.1. Reagents. All reactants were purchased from commercial suppliers and used as received. Ultrapure nitric acid (70 wt %, 15.9 M), produced by EuroChem (Novomoskovskiy Azot), was used in all cases. Pure palladium powder (99.99%) acid produced by “The Gulidov Krasnoyarsk Non-Ferrous Metals Plant” Open Joint Stock Company was used. The (R₄N)NO₃ (R = Me, Et, n-Pr, n-Bu) nitrate salts were prepared by the action of concentrated nitric acid on the corresponding bromide salts ((R₄N)Br, Acros Organics, 98%), recrystallized from H₂O/HNO₃ solutions, and dried in a stream of air.²³ Acetone was dried prior to use by means of the NaI solvate.²⁷ 1,10-Phenanthroline-5,6-dione was prepared according to the reported method.²⁸

Cerium dioxide was prepared by the thermal decomposition of Ce(NO₃)₆·6H₂O at 450 °C for 6 h in air. Ni(OH)₂ was precipitated from a solution of Ni(NO₃)₂ by the addition of NaOH and washed thoroughly with water and then with acetone, and the product was filtered off and dried in an air stream and then under vacuum for 24 h. SiO₂ (Polisorb, 220 m²/g), TiO₂ (Hombifine N, 320 m²/g), and Al₂O₃ (Pural TM80, 180 m²/g) were used as received.

2.2. Complex Preparation. **2.2.1. Preparation of the Salts (R₄N)₂[Pd(NO₃)₄] (R = Me (1), Et (2), n-Pr (3)).** Compounds 1–3 were synthesized using the procedure described below. Palladium powder (1 mmol) was dissolved in 3 mL of concentrated nitric acid with constant stirring. The solution was heated at 60 °C until NO₂ fumes ceased, the resulting solution was cooled to room temperature, and 3 mmol of the corresponding salt (R₄N)NO₃ (R = Me, Et, n-Pr) was then added. After complete dissolution of the salt, the solution was evaporated in an air stream to minimize the volume to about 0.75 mL. The crystalline product was filtered off and dried in an air stream before being washed with 25 mL of diethyl ether and then dried in an air stream. Due to the high solubility of the (R₄N)[Pd(NO₃)₄] salts, the yield mainly depends on the degree of solution evaporation and was about 80% in the described protocol. Single crystals of compounds 1–3 were picked directly from the nitric acid solutions.

2.2.1.1. (Me₄N)₂[Pd(NO₃)₄] (1). Anal. Calcd (found) for C₈H₂₄N₆O₁₂Pd: C, 19.11 (18.8); H, 4.81 (4.8); N, 16.72 (16.6). IR (cm⁻¹, KBr): 3046 (ν_{as}(CH₃)), 1495 (δ_{as}(CH₃)), 1412 (δ_s(CH₃)), 1510, 1484 (ν₅(NO₃)), 1251 (ν₁(NO₃)), 967 (ν₂(NO₃)), 946 (ν_{as}(C–N)), 797, 767 (ν₄(NO₃)).

2.2.1.2. (Et₄N)₂[Pd(NO₃)₄] (2). Anal. Calcd (found) for C₁₆H₄₀N₆O₁₂Pd: C, 31.25 (30.9); H, 6.56 (6.5); N, 13.67 (13.6). IR (cm⁻¹, KBr): 2989 (ν_{as}(CH₃)), 2954 (ν(C–H)), 1438 (δ_{as}(CH₃)), 1389 (δ_s(CH₃)), 1504, 1480 (ν₅(NO₃)), 1250 (ν₁(NO₃)), 975 (ν₂(NO₃)), 1002 (ν_{as}(C–N)), 789, 775 (ν₄(NO₃)).

2.2.1.3. (Pr₄N)₂[Pd(NO₃)₄] (3). Anal. Calcd (found) for C₂₄H₅₆N₆O₁₂Pd: C, 39.64 (39.2); H, 7.76 (7.4); N, 11.56 (11.5). IR (cm⁻¹, KBr): 2977 (ν_{as}(CH₃)), 2937 (ν_{as}(CH₂)), 2879 (ν_s(CH₃)), 1470 (δ_{as}(CH₃)), 1387 (δ_s(CH₃)), 1480 (ν₅(NO₃)), 1252 (ν₁(NO₃)), 980 (ν₂(NO₃)), 968 (ν_{as}(C–N)), 799 (ν₄(NO₃)).

2.2.2. Reactions of (Et₄N)₂[Pd(NO₃)₄] with N-Donor Ligands. To prepare complexes 4 and 5, 0.17 mmol of pyridinium nitrate

(pyHNO₃) or 0.085 mmol of 1,10-phenanthroline-5,6-dione (phd), correspondingly dissolved in 2 mL of acetone, was added to a freshly prepared solution of the salt 2 (50 mg, 0.081 mmol) in 1 mL of acetone. The mixture was stirred to obtain a clear solution and then evaporated to about 1.5 mL in an air stream and placed in a refrigerator (5 °C) for crystallization in a closed vial. After 40 min, the fine crystalline precipitates were filtered off with a porous PTFE membrane (0.22 μm), washed with acetone, and dried in an air stream. The yields were 85% (4) and 80% (5). Single crystals for an X-ray crystallographic study were picked directly from a mass of as-prepared products.

2.2.2.1. [Pd(py)₂(NO₃)₂] (4). Anal. Calcd (found) for C₁₀H₁₀N₄O₆Pd: C, 30.91 (30.9); H, 2.59 (2.6); N, 14.42 (14.1).

2.2.2.2. (Et₄N)[Pd(phd)(NO₃)₂NO₃·C₃H₆O] (5). Anal. Calcd (found) for C₂₃H₃₂N₆O₁₂Pd: C, 39.98 (40.2); H, 4.67 (4.5); N, 12.16 (12.0).

2.3. Apparatus. ¹⁵N NMR spectra were recorded at 50.7 MHz using an Avance III 500 Bruker spectrometer with a 5 mm broad-band probe. A 90° excitation pulse of 14 μs was applied. The spectra were recorded at −45 ± 0.2 °C. δ(¹⁵N) values (ppm) are reported relative to an external reference, a 1 M aqueous solution of Na¹⁵NO₃. The spectral window was about 600 Hz (10–12 ppm), and the delay between pulses was 100 s. ¹⁵N-enriched 10 M nitric acid (98 atom % ¹⁵N) (Sigma-Aldrich, 609323) was used for the solution preparation. An aliquot of the enriched nitric acid was mixed with a calculated volume of the Pd solution in concentrated naturally abundant nitric acid (15.9 M) to obtain 25 atom % ¹⁵N enrichment. To obtain integral intensities for the signals and evaluate the Pd species distribution, the ¹⁵N NMR spectra were fitted by the superposition of Voigt profiles as implemented in ACD/Laboratories NMR processor software (version 12.01).

Elemental CHN analysis was carried out on a Vario MICRO cube CHNS analyzer. The composition of Pd-Ni/SiO₂ catalysts was determined using micro beam X-ray fluorescence analysis on a M1MISTRAL Micro-XRF spectrometer (Bruker).

Differential thermal analysis of the salts 1–3 was carried out with a TG 209 F1 Iris instrument (NETZSCH) in a He (70 mL/min) stream at a heating rate of 10 °C/min.

Infrared spectra for tablets of KBr were recorded in the range of 400–4000 cm⁻¹ on a Scimitar FTS 2000 apparatus. Electron absorbance spectra of the solutions were recorded with a PG Instruments T60 UV–vis single-beam spectrophotometer; quartz cells with a 1 cm optical path length were used. Diffuse reflectance spectra were recorded in the 240–800 nm range with a Kolibri-2 compact multichannel spectrometer (VMK-Optoelektronika) equipped with a fiber optic cable (Ocean Optics, QR-400–7) and D/W lamp (Avalight-DHS). BaSO₄ powder was used as a reference.

Raman spectra were collected using a LabRAM HR Evolution (Horiba) spectrometer with excitation by the 514 nm line of an Ar⁺ ion laser. The spectra at room temperature were obtained in the backscattering geometry with a Raman microscope. The laser beam was focused to a diameter of 2 μm using a LMPlan FL 50x/0.50 Olympus objective. The spectral resolution was 3 cm⁻¹. The laser power on the sample surface was about 0.2 mW.

X-ray powder diffraction analysis of the polycrystalline samples was carried out on a DRON-RM4 diffractometer (Cu Kα radiation, graphite monochromator in the reflected beam, scintillation detector with amplitude discrimination). The samples were prepared by deposition of a suspension in hexane on the polished side of a cell made of fused quartz. A sample of polycrystalline silicon (*a* = 5.4309 Å), prepared similarly, was used as an external standard.

The structure and microstructure of the samples were studied by high-resolution transmission electron microscopy (TEM) using a ThemisZ electron microscope (Thermo Fisher Scientific, USA) with an accelerating voltage of 200 kV and a maximum lattice resolution of 0.06 nm. The device is equipped with a SuperX energy-dispersive X-ray spectrometer (EDX) (Thermo Fisher Scientific, USA) with a semiconductor Si detector with an energy resolution of 128 eV. For electron microscopy studies, sample particles were deposited on perforated carbon substrates attached to aluminum grids using the

ultrasonic dispersant UZD-1UCH2. Images were recorded using a Ceta 16 CCD sensor (Thermo Fisher Scientific, USA).

The XPS measurements of samples were performed on a SPECS (Germany) photoelectron spectrometer equipped with a PHOIBOS-150 hemispherical energy analyzer and Al K α irradiation ($h\nu = 1486.6$ eV, 200 W). The binding energy (BE) scale was precalibrated using the positions of the photoelectron of Au 4f $_{7/2}$ (BE = 84.0 eV) and Cu 2p $_{3/2}$ (BE = 932.67 eV) core level peaks. The residual gas pressure was better than 8×10^{-9} . The binding energy of peaks was calibrated by the position of the C 1s peak (BE = 284.7 eV) corresponding to the hydrocarbons present on the sample surface. Spectral analysis and peak fitting were performed with XPSPeak 4.1 software. Integral intensities of the spectra were corrected by their respective atomic sensitivity factors.²⁹

2.4. X-ray Crystallographic Data Collection and Refinement.

Crystal data and experimental details for compounds 1–3 and 5 are given in Table S1 in the Supporting Information. Experimental data for the determination of the crystal structures of 1 and 4 were collected on a Bruker D8 Venture diffractometer, while a Bruker APEX-II CCD diffractometer at 150 K with graphite-monochromated Mo K α radiation ($\lambda = 0.7107$ Å) was used for the crystal structures of 2, 3, and 5. All calculations were carried out with the SHELX-97 crystallographic software package.³⁰ The structures were solved by the standard heavy-atom method and refined by the anisotropic approximation. The H atoms were refined in their geometrically calculated positions; a riding model was used for this purpose. Absorption corrections were applied empirically using the SADABS software.³¹ A Hirshfeld molecular surface analysis was performed using the Crystal Explorer 3.1 program.³²

CCDC 2026407 (1), 2025660 (2), 2008746 (3), and 2026628 (5) contain the supplementary crystallographic data for this paper. These data can be obtained free of charge from the Cambridge Crystallographic Data Centre via www.ccdc.cam.ac.uk/data_request/cif.

2.5. Density Functional Theory (DFT) Calculations. Geometry optimization was carried out using the Gaussian 09C software package.³³ Structures of [Pd(NO $_3$) $_4$] $^{2-}$ anions from X-ray crystallographic data were used as initial states. The calculations were performed using the B3LYP^{34–37} method and the LANL2DZ^{38–42} basis set for entire molecules placed in a cavity within the water reaction field (SCRFF solvent method⁴³). The calculations of IR frequencies showed no imaginary vibrations, emphasizing that the local minima were achieved in all cases. The rigid PES scans for rotation of the nitrate group were performed by the following procedure: the dihedral angle O–Pd–O–N was modified from 152 to -14° with a 2 or 4 $^\circ$ step, and single-point calculations were performed at each point.

The relaxed potential energy surface scans (PES scans) for transformations between two modifications of [Pd(NO $_3$) $_4$] $^{2-}$ (an outer-sphere mechanism) and also for substitution of one nitrate ligand with water or acetone were performed with the ADF-2016 software package using the TZP basis set for all atoms and the B3LYP functional. Water, chosen as a solvent, was modeled with the COSMO method. The relativistic effects were taken into account with a scalar zero-order relativistic approximation (ZORA). The scans were performed by the following scheme: the substituent from the outer sphere of [Pd(NO $_3$) $_4$] $^{2-}$ (NO $_3^-$, H $_2$ O, or acetone) was moved to palladium atom by an oxygen atom; therefore, the Pd–O distance decreased from 5.0 to 2.1 Å (the last distance is close to the equilibrium Pd–O distance). The geometry was optimized at each point of the scan. Also, the geometry of the final state ([Pd(NO $_3$) $_3$ (L)] $^{n-}$, L = NO $_3^-$, H $_2$ O, or acetone, $n = 1, 2$) and NO $_3^-$ was optimized in two independent calculations modeling the situation when nitrate was moved far away from the obtained complex, and the sum of the two energies ($E([\text{Pd}(\text{NO}_3)_3(\text{L})]^{n-}) + E(\text{NO}_3^-)$) was used for plotting.

The calculations of the electron localization function (ELF) for all isomers were performed with the ADF-2016⁴⁴ software package, using the TZP basis set for all atoms and the B3LYP^{34–37} functional. Water, chosen as a solvent, was modeled with the COSMO⁴⁵ method. The

relativistic effects were taken into account with a scalar zero-order relativistic approximation (ZORA).

2.6. Pd Sorption on Supporting Materials. The general procedure described below was used to study the ability of Al $_2$ O $_3$, CeO $_2$, TiO $_2$, SiO $_2$, and Ni(OH) $_2$ to chemisorb palladium species from solutions of the complexes (R $_4$ N) $_2$ [Pd(NO $_3$) $_4$]. Oxides were calcined prior to use at 150 $^\circ$ C under vacuum for 24 h; Ni(OH) $_2$ was also treated under vacuum at room temperature for 24 h. Then, 100 mg of the appropriate solid material was added to a freshly prepared 10 mM solution of (R $_4$ N) $_2$ [Pd(NO $_3$) $_4$] in 1.5 mL of dry acetone in a 3 mL vial, and the mixture was stirred vigorously. The resulting suspension was centrifuged at 4000 rpm, and the color of the supernatant was visually checked. Additionally, the completeness of the uptake was confirmed by UV–vis spectrophotometry at 380 nm. To evaluate the maximum uptake for a given material, the protocol described above was repeated with solutions of variable Pd concentrations.

2.7. Preparation of the Pd-Ni/SiO $_2$ Catalyst. Nickel nitrate was dissolved in acetone, and 3 g of SiO $_2$ was then added. The resulting suspension was stirred for 15 min, and the solvent was then removed in an air stream with constant stirring. The resulting solid product was poured into 100 mL of a 0.2 M NaOH aqueous solution, and the suspension was stirred for 30 min. The solid product was isolated by centrifugation, washed with water up to the supernatant pH 7, and then washed three times with acetone and dried under vacuum for 24 h. The Ni(OH) $_2$ /SiO $_2$ composite obtained was redispersed in acetone, and a solution of salt 2 (300 mg) in 5 mL of acetone was added to the suspension, with constant stirring. After 10 min of stirring, the solid material was isolated by filtration on a PTFE membrane (0.22 μ m), washed with 50 mL of acetone, and dried in an air stream. The resulting solid material was calcined at 200 $^\circ$ C in an air atmosphere and then reduced at 400 $^\circ$ C in a stream of pure hydrogen (30 min).

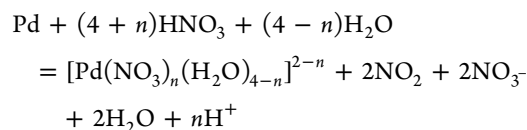
2.8. Catalytic Hydrazine Decomposition over Pd-Ni/SiO $_2$ Catalyst. The release of a gaseous product during the catalytic decomposition of hydrazine hydrate was carried out using an installation that includes a closed 10 mL vial connected to a gas buret. The temperature of the vial was maintained with a thermostated water jacket. In a typical procedure, the as-prepared catalyst (300 mg) was placed in the vial and dispersed in 1 mL of 1 M NaOH. The vial was then closed and connected to a buret. The reaction was initiated by injection of hydrazine hydrate (25 μ L, 0.463 mmol of N $_2$ H $_4$; the exact concentration was determined by an acid–base titration with methyl red indicator) to the suspension in the vial. The volume of evolved gases (N $_2$ + H $_2$) was monitored using a water replacement method. Water in the trap was acidified with H $_2$ SO $_4$ to ensure complete NH $_3$ capture. The selectivity (α) and turnover frequency (TOF) values were calculated in accordance with the formulas

$$\alpha = (3\lambda - 1)/8 \quad \text{where } \lambda = n(\text{N}_2 + \text{H}_2)/n(\text{N}_2\text{H}_4)$$

$$\text{TOF} = n(\text{H}_2)/(n(\text{Pd}) \times t)$$

3. RESULTS AND DISCUSSION

3.1. Synthesis and Properties of the Salts (R $_4$ N) $_2$ [Pd(NO $_3$) $_4$]. Dissolution of metallic palladium in nitric acid results in the formation of the palladium(II) aqua-nitratocomplex series:^{46,47}



As reported previously, in concentrated nitric acid solution (above 13 M), the anionic species [Pd(NO $_3$) $_n$ (H $_2$ O) $_{4-n}$] $^{2-n}$ with $n = 3, 4$ dominate.^{47,48} A fast ligand exchange around the Pd centers was observed in such solutions, but direct

speciation studies using ^{15}N NMR are possible at low temperatures (below $-40\text{ }^\circ\text{C}$). The typical ^{15}N NMR spectrum of the Pd nitric acid solution, which was used to prepare the $(\text{R}_4\text{N})_2[\text{Pd}(\text{NO}_3)_4]$ salts, is shown in Figure 1. From a fitting

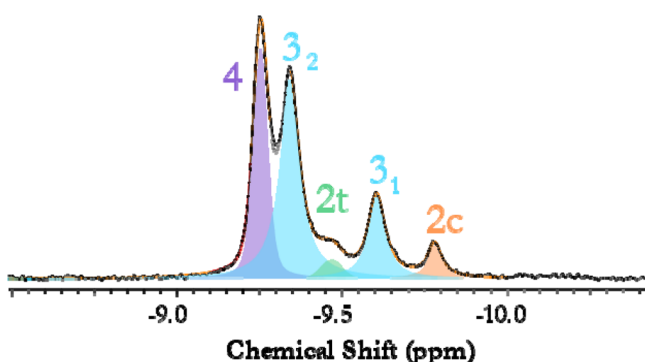


Figure 1. ^{15}N NMR spectrum of a palladium nitric acid solution ($C(\text{Pd}) = 0.33\text{ M}$ and $C(\text{HNO}_3) = 13.5\text{ M}$) at $-45\text{ }^\circ\text{C}$. The signals are assigned according to previous data.⁴⁷ Legend: 4, $[\text{Pd}(\text{NO}_3)_4]^{2-}$; 3₂ and 3₁, $[\text{Pd}(\text{NO}_3)_3(\text{H}_2\text{O})]^-$; 2t, *trans*- $[\text{Pd}(\text{NO}_3)_2(\text{H}_2\text{O})_2]$; 2c-*cis*- $[\text{Pd}(\text{NO}_3)_2(\text{H}_2\text{O})_2]$.

of the spectrum with a superposition of Voigt profiles, the next fraction of the species can be calculated: 27% $[\text{Pd}(\text{NO}_3)_4]^{2-}$, 56% $[\text{Pd}(\text{NO}_3)_3(\text{H}_2\text{O})]^-$, 8% *trans*- $[\text{Pd}(\text{NO}_3)_2(\text{H}_2\text{O})_2]$, and 9% *cis*- $[\text{Pd}(\text{NO}_3)_2(\text{H}_2\text{O})_2]$.

Evaporation of a nitric acid solution of palladium (13–16 M HNO_3 , $C(\text{Pd}) = 0.33\text{ M}$) with an excess of the corresponding $(\text{R}_4\text{N})\text{NO}_3$ ($\text{R} = \text{Me}, \text{Et}, \text{Pr}$) salt results in the formation of salts $(\text{R}_4\text{N})_2[\text{Pd}(\text{NO}_3)_4]$ (1–3). Fast evaporation leads to the precipitation of small, badly shaped crystals (Figure 2a–c),

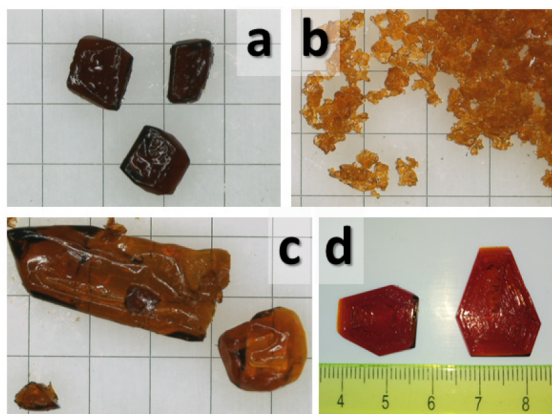


Figure 2. Photographs depicting the typical morphologies of salts 1 (a), 2 (b) and 3 (c), obtained by fast evaporation, and large crystals of 2 (d), grown by slow evaporation of the solution in a Petri dish. The graduation for (a)–(c) is 1 mm; the linear size is given in centimeters in (d).

while slow evaporation of the solutions, especially in a thin layer (Petri dish), allows large well-edged pinacoids (Figure 2d) to grow. Attempts were also made to prepare a salt with a tetrabutylammonium cation (Bu_4N^+) in an analogous manner, but these were without success: after evaporation, an oily mass was formed that did not transform into a crystalline product, even under freezing conditions.

X-ray powder diffraction analysis of the obtained solid products 1–3 shows good agreement with the single-crystal

data that confirms their phase homogeneity (Figure S1). In the infrared spectra of the prepared salts 1–3, the series of strong bands observed at about 1500, 1250, 970, and 790 cm^{-1} (Figure S2) correspond to the ν_5 , ν_1 , ν_2 , and ν_4 vibrations of coordinated NO_3^- ions.⁴⁹ The overall position of the signals is consistent with the unidentate coordination mode of the nitrate ligand.⁵⁰ The frequency of the ν_5 band is considerably lower than the position of the corresponding bands reported for $[\text{Au}(\text{NO}_3)_4]^-$ and $[\text{Pt}(\text{NO}_3)_6]^{2-}$ anions,^{23,51} which implies a lower polarization degree of NO_3^- by Pd^{2+} ions. Interestingly, a close ν_5 band frequency value was found for a rhodium(III) complex salt containing a mixture of the *trans*- $[\text{Rh}(\text{H}_2\text{O})_2(\text{NO}_3)_4]^-$ and $[\text{Rh}(\text{NO}_3)_6]^{3-}$ nitrate complexes.⁵² Raman spectra of the salts 1–3 were also studied (Figure S3). Aside from signals corresponding to the R_4N^+ cations, which were deduced by comparison with the spectra of the corresponding chlorides (R_4NCl), strong bands at 320, 725, 780, and 995 cm^{-1} can be found that are attributed to the stretching and bending vibrations of Pd- ONO_2 groups. The positions of these signals are also in agreement with values reported for salts containing the $[\text{Au}(\text{NO}_3)_4]^-$ anion.⁵¹

3.2. Reactivity of the Salts. The salts 1–3 are not hygroscopic, and both the bulk crystals and powders can be stored in open containers for prolonged periods (>1 year) without notable moisture uptake. On the other hand, on dissolution of the salts in water, hydrolysis proceeds almost immediately. As evidenced from UV–vis spectra of the resulting yellow solutions (Figure 3A), $[\text{Pd}(\text{NO}_3)_4]^{2-}$ anions are almost completely aquated, and the palladium(II) aqua ion (380 nm , $\epsilon = 80$)^{53,54} dominates, accompanied by only traces of the aqua nitrate species. An additional weak band at 301 nm corresponds to the absorption of the free nitrate ion.⁵⁵

The salts can also be easily dissolved in acetone, THF, and acetonitrile, but they are insoluble in toluene, hexane, dioxane, ethyl acetate, and diethyl ether. On dissolution in organic solvents, rapid solvolysis proceeds, accompanied by a color change from brown to yellow and the corresponding changes in the UV–vis spectra (Figure 3B). In addition to the long-wave band at 450 nm , which is characteristic for d–d transitions in nitrate complexes of Pd(II),^{46,53,54} a strong band arises at about 380 nm , corresponding to a ligand to metal charge transfer. Such changes, by analogy with the spectral changes observed during the aquation process, can be attributed to the substitution of nitrate ligands by organic solvent molecules S, leading to the formation of $[\text{Pd}(\text{S})_n(\text{NO}_3)_{4-n}]^{n-2}$ species.

The prepared salts 1–3 possess sufficient thermal stability and do not decompose up to $200\text{ }^\circ\text{C}$ (Figure 4), which is in contrast with palladium nitrate ($[\text{Pd}(\text{NO}_3)_2(\text{H}_2\text{O})_2]$), which starts to decompose below $100\text{ }^\circ\text{C}$. Above $200\text{ }^\circ\text{C}$, fast decomposition of the salts occurs, with the formation of metallic palladium and amorphous carbon. An interesting peculiarity is the melting of salts 1–3 at about $190\text{ }^\circ\text{C}$, just before decomposition begins. Melting is accompanied by a notable endothermic effect on the DTA curve (Figure S4), while further decomposition to Pd metal is highly exothermic, corresponding to the reaction between nitrate ligands and organic cations. It should be noted that the decomposition of the salts proceeds smoothly without any explosion or ignition, which is in agreement with the general rule that strong oxidizing properties are observed only for nitrate complexes containing bidentate nitrate groups.^{50,56} After complete decomposition of the salts 1–3, a slow mass growth is

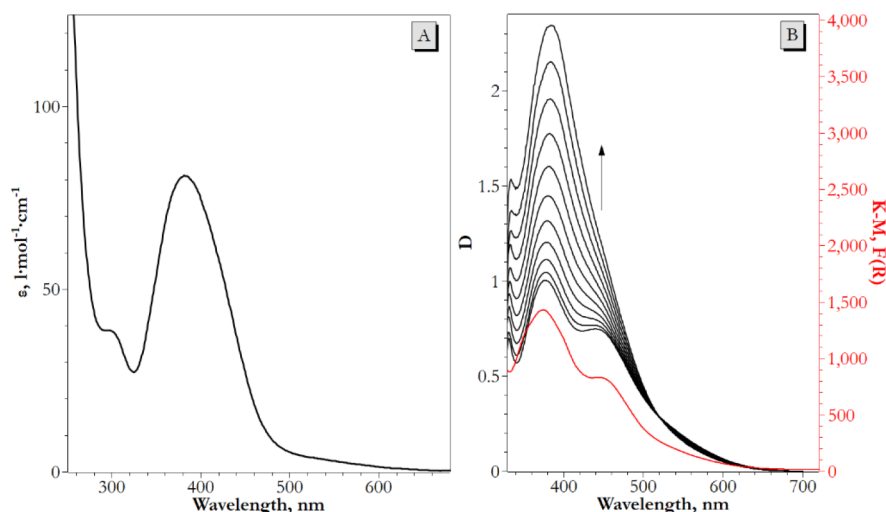


Figure 3. (A) UV-vis spectrum of salt **2** in 0.2 M HClO₄. (B) Evolution of the UV-vis spectrum of the salt **2** solution in acetone ($C(\text{Pd}) = 5.2$ mM). The diffuse reflectance spectrum of **2** is additionally presented (red line) for comparison.

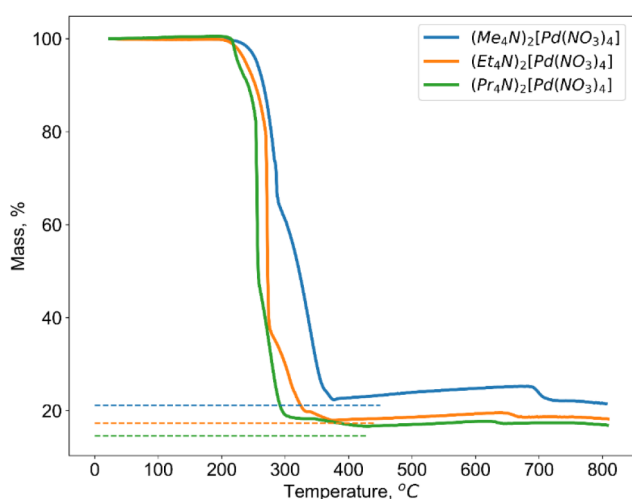


Figure 4. TG curves depicting the thermal decomposition of salts **1–3** in He. The dashed lines mark the calculated weight loss corresponding to the complete decomposition of the salt to Pd metal.

observed above 350 °C, which corresponds to Pd oxidation with the trace oxygen present in the helium stream. At temperatures above 650 °C, the formed PdO becomes unstable and decomposes back into metallic Pd and oxygen.¹⁹

3.3. Crystal Structures. The structures of salts **1–3** are built from $[\text{Pd}(\text{NO}_3)_4]^{2-}$ complex anions and R_4N^+ cations, packed without any solvent molecules into monoclinic unit cells in the case of salts **1** and **3** ($P2_1/n$ and $P2_1/c$ space groups, correspondingly) and a tetragonal ($I4/mmm$) cell in the case of the tetraethylammonium salt **2**. Increasing the organic cation size leads to a decrease in the number of cations surrounding the complex anions, from 12 in the case of salt **1** (Me_4N^+) to 9 for salt **2** (Et_4N^+) and 8 for salt **3** (Pr_4N^+). As evidenced from an analysis of Hirshfeld surfaces (Table 1) for anions and cations in the structures of **1–3**, elongation of the R alkyl chain from CH_3 to $n\text{-C}_3\text{H}_7$ also results in an increase in the $\text{O}\cdots\text{H}$ contact fraction for $[\text{Pd}(\text{NO}_3)_4]^{2-}$ anions, from 86% to 93%. In agreement with this, the fraction of $\text{O}\cdots\text{O}$ contacts on the Hirshfeld surfaces of complex anions, corresponding to the contacts between neighboring anions, falls from 5% for salt **1** to almost 0 in the case of salt **3**. An analogous trend is also

Table 1. Hirshfeld Surface Analysis of Complex Salts **1–3**

$(\text{Me}_4\text{N})_2[\text{Pd}(\text{NO}_3)_4]$ (1)						$(\text{Et}_4\text{N})_2[\text{Pd}(\text{NO}_3)_4]$ (2)					
anion (γ)		cation (1)		cation (2)		anion (α)		cation (1)		cation (2)	
Pd–H	0.2	H–Pd	0.3	H–Pd	0.1	Pd–Pd	1.0	H–O	53.0	H–O	39.9
N–O	2.0	H–O	63.4	H–O	61.1	Pd–O	0.1	H–N	5.0	H–N	0.4
O–N	1.6	H–N	2.7	H–N	3.9	O–Pd	0.1	H–H	42.0	H–H	59.7
O–O	4.9	H–H	33.6	H–H	34.9	O–O	2.8				
O–H	86.5					O–H	90.5				
N–H	4.8					N–H	5.5				
$(\text{Pr}_4\text{N})_2[\text{Pd}(\text{NO}_3)_4]$ (3)											
anion (β)		anion (γ)		cation (1)		cation (2)		cation (1)		cation (2)	
Pd–H	1.2	Pd–H	0.2	H–Pd	0.2	H–Pd	0	H–Pd	0.2	H–Pd	0
O–H	92.7	O–H	93.2	H–O	33.6	H–O	33.8	H–O	33.6	H–O	33.8
N–H	6.0	N–H	6.6	H–N	3.5	H–N	3.5	H–N	3.5	H–N	3.5
				H–H	62.7	H–H	62.7	H–H	62.7	H–H	62.7

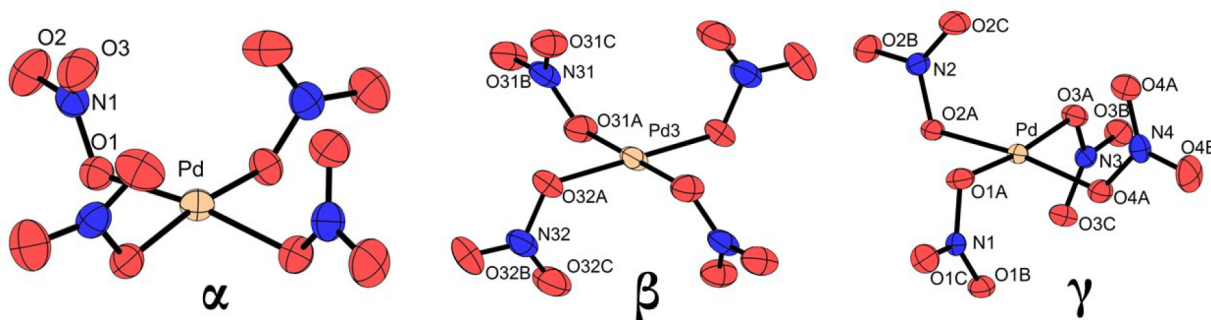


Figure 5. Structure of α , β , and γ modifications of the complex anion $[\text{Pd}(\text{NO}_3)_4]^{2-}$: the α form from the structure of **2**, the β form from the structure of **3**, and the γ form from the structure of **1**.

observed for N...O contacts. Such tendencies indicate that bulk R_4N^+ cations form voids around the complex anions $[\text{Pd}(\text{NO}_3)_4]^{2-}$ and separate them from each other. A similar isolation of complex anions was described for the platinum(IV) nitrate complexes $[\text{Pt}(\text{NO}_3)_6]^{2-}$ and $[\text{Pt}_2(\mu\text{-OH})_2(\text{NO}_3)_8]^{2-}$ with R_4N^+ cations, where $\text{R} = n\text{-Pr}, n\text{-Bu}$.²³

The palladium center of the $[\text{Pd}(\text{NO}_3)_4]^{2-}$ anions possesses a distorted-square-planar geometry with four NO_3^- ligands coordinated in a unidentate mode. In all cases, Pd–O bonds are practically identical (2.00–2.01 Å), as are the O–Pd–O angles, which are close to 90°. A general peculiarity of the $[\text{Pd}(\text{NO}_3)_4]^{2-}$ structure is two possible arrangements of the NO_3 ligands with respect to the PdO_4 plane, above and below (Figure 5); therefore, four different isomers of this anion can be assumed. Two isomers, designated as α and β modifications, were previously reported by Khramenko et al. in the structures of the salts with alkali-metal cations.^{20–22,57} α - $[\text{Pd}(\text{NO}_3)_4]^{2-}$ comprises four nitrate ligands situated on one side of the PdO_4 plane; in the structure of β - $[\text{Pd}(\text{NO}_3)_4]^{2-}$, two nitrate ligands situated in positions *cis* to each other are located on one side of the PdO_4 plane and the other two ligands are on the opposite side, forming a chairlike structure.

In the structure of salt **1**, a previously unreported form of the $[\text{Pd}(\text{NO}_3)_4]^{2-}$ anion was found, which we have designated the γ modification. Two nitrate ligands of γ - $[\text{Pd}(\text{NO}_3)_4]^{2-}$, located in positions *trans* to each other, are situated on one side of the PdO_4 plane, while the other two are located on the opposite side (Figure 5 and Table S2). Interestingly, the N(1)O₃ and N(3)O₃ ligands are located practically in one plane, whereas the ligands with N2 and N4 atoms are rotated with respect to each other, at 22°. The system of weak hydrogen bonds (2.4–2.5 Å) with the nearby tetramethylammonium cation is also observed in the structure (Figure S5).

The basketlike structure of the α - $[\text{Pd}(\text{NO}_3)_4]^{2-}$ anion in the crystal structure of salt **2** (Figure 5 and Table S3) is almost identical with that described previously in $\text{KCs}[\text{Pd}(\text{NO}_3)_4] \cdot 0.5\text{H}_2\text{O}$ and $\text{K}_2[\text{Pd}(\text{NO}_3)_4]$ salts^{21,22} and can also be compared with the structure of the polar $[\text{Pd}(\text{IO}_3)_4]^{2-}$ complex.⁵⁸ The nitrate ligands of the α - $[\text{Pd}(\text{NO}_3)_4]^{2-}$ anion are turned in one direction, and in the structure of **2**, pairs of anions with different directions of ligand rotation are arranged side by side, with a Pd...Pd distance of about 3.2 Å (Figure S6A). The disorder of the positions of nitrate ligands and tetraethylammonium cations is observed in the structure, and all eight complex anions in the cell are located on a 4-fold axis (Figure S6B).

The structure of salt **3**, with a tetrapropylammonium cation, contains four crystallographically independent $[\text{Pd}(\text{NO}_3)_4]^{2-}$

anions of the β and γ modifications. Complex anions of the β modification are located on the inversion centers, whereas the remaining γ - $[\text{Pd}(\text{NO}_3)_4]^{2-}$ anions are arranged along the 2-fold helical axes. The organic cations are situated on glide planes. The structure of β - $[\text{Pd}(\text{NO}_3)_4]^{2-}$ is similar to that of the previously described β - $\text{K}_2[\text{Pd}(\text{NO}_3)_4]$ (Figure 5 and Table S4), and the structure of γ - $[\text{Pd}(\text{NO}_3)_4]^{2-}$ in complex salt **3** is almost the same as that in case **1** (Table S4).

It is interesting to note that one of the possible isomers of the $[\text{Pd}(\text{NO}_3)_4]^{2-}$ complex, featuring one nitrate ligand rotated in the opposite direction with respect to the other three ligands (designated further as the δ isomer), has not been observed in the crystal structures to date. To investigate the electronic structure of the $[\text{Pd}(\text{NO}_3)_4]^{2-}$ complexes, to determine how the isomers are ranged by electronic energy, and to figure out the possibility of their interconversion, we proceeded further with DFT calculations.

3.4. DFT Calculations. The DFT-optimized structures of each type of $[\text{Pd}(\text{NO}_3)_4]^{2-}$ complex (α , β , γ) are close to those found from crystallographic data, and no serious changes in geometry were observed during the optimization. This observation highlights that the electron energies of α , β , and γ complexes observed in the crystal structure of salts **1–3** correspond to local minima on the potential energy surface. Additionally, the δ isomer of the $[\text{Pd}(\text{NO}_3)_4]^{2-}$ complex was considered, which has not been observed in the crystal structures of the isolated compounds (Figure 6). Among all of the isomers, the α - $[\text{Pd}(\text{NO}_3)_4]^{2-}$ has the minimum electron energy and was chosen as a reference ($E = 0$ kJ/mol) for comparison. In this reference frame, the electron energies of β - $[\text{Pd}(\text{NO}_3)_4]^{2-}$ and δ - $[\text{Pd}(\text{NO}_3)_4]^{2-}$ isomers are 1.24 and 1.71 kJ/mol, respectively, while the highest energy value (4.98 kJ/

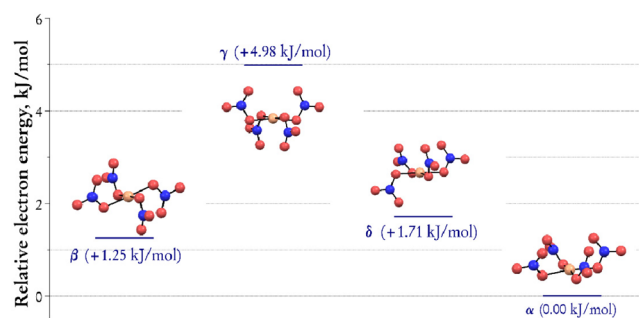


Figure 6. DFT optimized structures of $[\text{Pd}(\text{NO}_3)_4]^{2-}$ isomers and their relative electronic energies.

mol) was calculated for the γ -[Pd(NO₃)₄]²⁻ species (Figure 6).

Several intense bands around 925, 1200, and 1390 cm⁻¹ were observed in the DFT-calculated IR spectra of [Pd(NO₃)₄]²⁻ anions (Figure S7), related to vibrations of the coordinated nitrate. Interestingly, some vibrations of N–O bonds are overlapped in the case of α and γ isomers, which is consistent with the high symmetry of these ions. The bands corresponding to vibrations of Pd–O bonds are located close to 340 and 700 cm⁻¹, but the intensities of these bands are more than 5 times weaker than those of the N–O vibrations. The calculated wavenumber values are generally in agreement with the experimental values, except for the ν_3 bending band of NO₃⁻ ligands, which is observed at about 100 cm⁻¹ higher wavenumber.

Figure S8 demonstrates the ELF in [Pd(NO₃)₄]²⁻ complexes, calculated in the cut planes formed with palladium and bonded oxygen atoms. Electrons are seen to be localized around the PdO₄ core almost symmetrically, even in the case where the nitrate ligand is rotated by 180°. The ELF around the aforementioned atoms is also seen to repeat the shape of the outer orbitals of oxygen (p orbitals) and palladium (d orbitals), which means that the s orbitals of oxygen only take part in σ bonds in nitrate ligands, and the π system of the nitrate ligand does not take part in the formation of Pd–O bonds. The localization of electrons over oxygen atoms is more diffuse than for palladium, which is related to the large difference in atomic charges of the atoms.

The differences between electronic energy values for α -[Pd(NO₃)₄]²⁻, β -[Pd(NO₃)₄]²⁻, and δ -[Pd(NO₃)₄]²⁻ isomers are lower than that of RT under normal conditions; therefore, the tetranitratopalladate anion can switch between these structures under ambient conditions if the energy barriers for these transformations are low enough. To analyze this possibility, we performed the calculations for the interconversion of α -[Pd(NO₃)₄] to δ -[Pd(NO₃)₄]²⁻, conducting a rigid PES scan for one O–Pd–O–N dihedral angle, while the other bonds and angles were kept constant. This situation imitates the possible transformation of α -[Pd(NO₃)₄] to δ -[Pd(NO₃)₄]²⁻ by the rotation of the nitrate ligand around the Pd–O bond. The resulting energy profile, described in Figure 7, clearly shows that there is a relatively high barrier of about 95 kJ/mol for the switch from α -[Pd(NO₃)₄] to δ -[Pd-

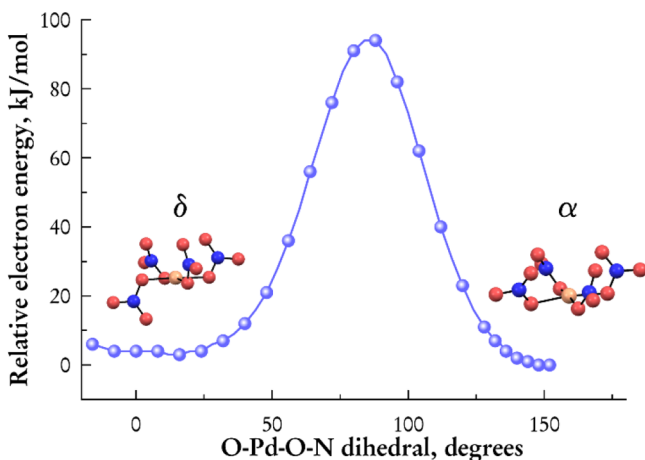
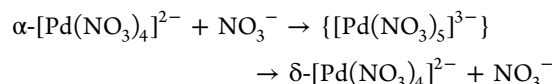


Figure 7. Rigid PES scan of the O–Pd–O–N dihedral angle during interconversion of α - to δ -[Pd(NO₃)₄]²⁻.

(NO₃)₄]²⁻ structures, with the transition state having the rotated NO₃ ligand aligned in the {PdO₄} plane.

In a nitric acid solution, on the other hand, due to the substitutional lability of palladium(II) complexes,^{59,60} the outer-sphere mechanism should definitely operate as well, including the formation of five-coordinated intermediates:



The relaxed PES scan was performed to model the given outer-sphere mechanism of transformation. The maximum energy in PES is related to the five-coordinated complex {[Pd(NO₃)₅]³⁻} with Pd–O distances of 2.2 Å, and an energy barrier of 85 kJ/mol is observed. Despite the limitations of the chosen calculation method, the energy of the transition state, in this case, is lower than that calculated for the rotation of NO₃⁻, confirming the hypothesis of the outer-shell transformation mechanism.

We also calculated relaxed PES scans for substitution of the nitrate ligand by water or acetone to illustrate the lability of the nitrate complex toward such reactions. The calculations were performed in the same manner as for the NO₃⁻ exchange reaction. In both cases, the incoming ligand (acetone, water) approaches the Pd atom by an O atom until the Pd–O distance is decreased to about 2.1 Å (average Pd–O distance), which refers to the maximum in PES (Figure S9). After this, the five-coordinated complex decomposes, forming free NO₃⁻ ion and the [Pd(NO₃)₃(L)]ⁿ⁻ complex (L = H₂O, acetone). The energy barriers are 72 and 85 kJ/mol for acetone and water, respectively, which is quite close to that found for NO₃⁻ exchange. It should be noted that the models chosen are the simplest ones; therefore, the energies obtained from the relaxed PES scans may be overestimated, resulting in the sharp shape of the plots.

3.5. Reaction with N-Donor Ligands. As evidenced from the study of [Pd(NO₃)₄]²⁻ anion reactivity in water and organic solvents, the nitrate ligands can be easily substituted by various species. To illustrate this peculiarity, we studied the interaction of salt **2** with two different N-donor ligands, pyridine (**py**) and 1,10-phenanthroline-5,6-dione (**phd**), in acetone. Palladium complexes with such types of ligands are of interest in antitumor therapy, as a building block for the synthesis of heterometallic complexes, and as synthetic metalloproteases.^{17,61,62}

The addition of **py** or **phd** to a freshly prepared solution of **2** leads to an immediate color change from brown to yellow and the gradual formation of a fine crystalline precipitate. The products, obtained in high yield, are the molecular complex *trans*-[Pd(**py**)₂(NO₃)₂] (**4**) and the adduct (Et₄N)[Pd(**phd**)(NO₃)₂](NO₃)·C₃H₆O (**5**), respectively. The formation of Pd(**py**)₂(NO₃)₂ in the *trans* form can be attributed to the much stronger *trans* influence of the **py** ligand in comparison with the nitrate ligands, while the geometry is dictated by the structure of the bidentate ligand in the case of *cis*-[Pd(**phd**)(NO₃)₂].

The crystal structure data for complex **4** have already been deposited in the structure database (CSD 1001419), but the synthesis and description of the structure have not been presented in the literature. Complex **4** crystallizes in the triclinic space group $P\bar{1}$ ($Z = 2$) without solvent molecules. There are two crystallographically independent Pd centers in the structure, both located on inversion centers and arranged

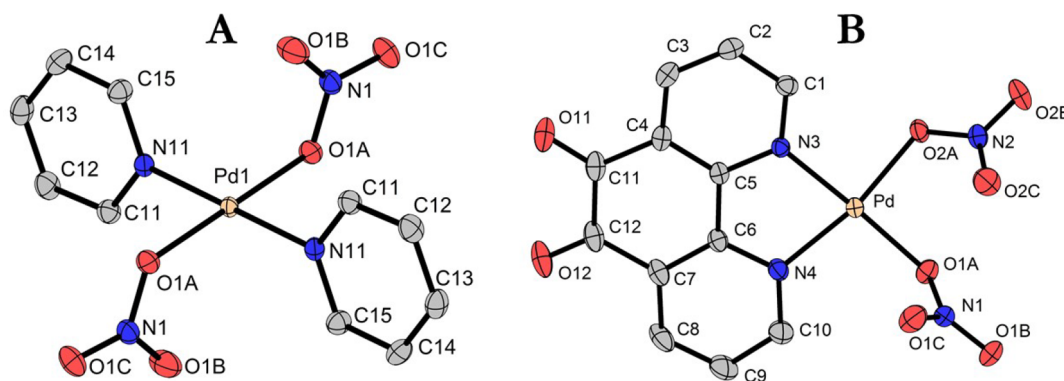


Figure 8. (A) Structure of *trans*-[Pd(py)₂(NO₃)₂] (4). (B) Structure of the [Pd(phd)(NO₃)₂] complex in the crystal structure of the adduct 5.

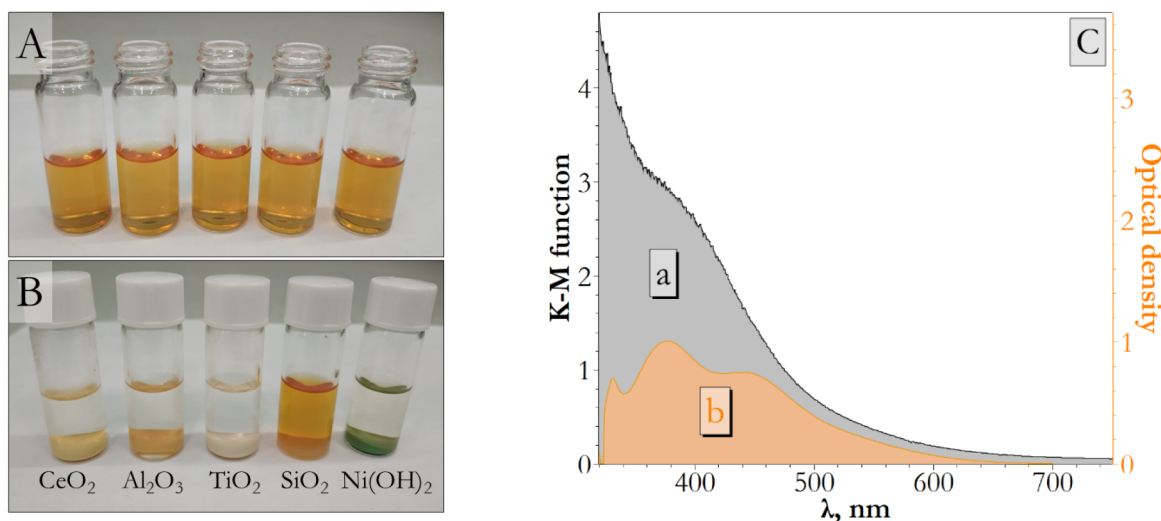


Figure 9. Solution of 2 in acetone ($C_{\text{Pd}} = 12 \text{ mM}$) before (A) and after the addition of CeO₂, Al₂O₃, TiO₂, SiO₂, and Ni(OH)₂ solids (100 mg) (B). (C) Diffuse reflectance spectrum of the palladium species deposited on Al₂O₃ (a) along with the UV-vis spectrum of the acetone solution of salt 2 (b).

into chains that run along all axes (Figure S10). The palladium atom in *trans*-[Pd(py)₂(NO₃)₂] coordinates in a square-planar manner, without notable distortions (Figure 8A), and Pd–O and Pd–N bonds are close—2.01–2.02 Å (Table S5). The organic ligands are situated in positions *trans* to each other and are practically coplanar, while the planes of the NO₃ ligands are parallel to each other.

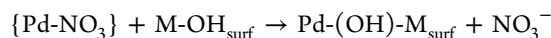
The neutrally charged complex [Pd(phd)(NO₃)₂] with 1,10-phenanthroline (phd) crystallizes in the triclinic space group $P\bar{1}$, along with the tetraethylammonium cation from the parent salt 2, the nitrate anion, and acetone, which was used as a solvent (Figure S11). In the structure of 5, two molecules of [Pd(phd)(NO₃)₂] are arranged around the center inversion in the middle part of the cell. The palladium atom has a distorted-square-planar environment formed by two oxygen atoms from the nitrate ligands and two nitrogen atoms from phd. The Pd–O bond lengths are 2.01–2.03 Å, and the Pd–N bond lengths are about 2.00 Å (Table S6). Due to the tough geometry of heteroaromatic rings, the N3–Pd–N4 angle differs sufficiently from 90° (81.7°). Also, note that N3, N4 and O1A atoms lie practically in one plane, but the O2A atom is located out of this plane; as a result, the O1A–Pd–N3 and O2A–Pd–N4 angles are noticeably different.

Compounds 4 and 5 are both almost insoluble in acetone, ethanol, and ether but can be readily dissolved in solvents

whose molecules are strongly bound ligands (acetonitrile, water, DMF), presumably accompanied by nitrate ligand substitution that is evidenced from ESI-MS data (Figures S12 and S13). Such lability of the nitrate ligands in 4 and 5 or analogous related compounds can be further exploited to prepare heteroleptic palladium(II) complexes or polynuclear frameworks.

3.6. Pd Deposition on Oxide or Hydroxide Supports.

As mentioned in the Introduction, the supported palladium catalysts are intensively used in various fields, and the development of facile methods and precursors for the preparation of such materials is an important task. Previously, we have reported on a labile polynuclear platinum(IV) nitrate complex that can be chemisorbed onto ceria or alumina materials by means of nitrate ligand substitution and the binding of platinum ions with –OH groups on the surface of the oxide.²³ In this context, a combination of the stability of salts 1–3 and lability of the [Pd(NO₃)₄]²⁻ species toward ligand substitution can be applied to the deposition of palladium species onto various solid supports that have reactive donor groups on the surface:



Indeed, the experiments with Al₂O₃ and CeO₂ have shown that a fast uptake of palladium takes place from the solution upon

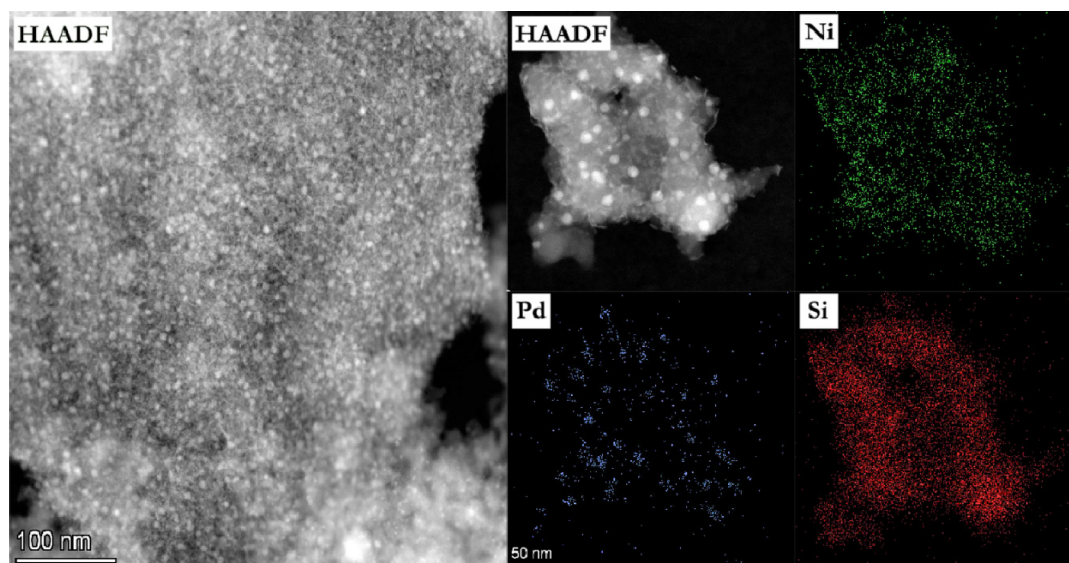


Figure 10. HAADF-STEM photographs of the $\text{Ni}_{0.9}\text{Pd}_{0.1}/\text{SiO}_2$ catalyst combined with the elemental mappings showing the spatial distribution of Ni, Pd, and Si.

addition of these oxides to acetone solutions of salts 1–3, which is evident from the discoloring of the supernatant and the color change of the solids (Figure 9A,B). Diffuse reflectance spectra of the materials with sorbed Pd species consist of a broad band at about 400 nm, which correlates with the position of the bands observed in spectra of the salt 2 acetone solution (Figure 9C). Unlike the case of platinum complexes, the sorption process for $[\text{Pd}(\text{NO}_3)_4]^{2-}$ anion salts proceeds extremely quickly: generally, almost immediately after the oxides are suspended. The sorption is irreversible, and deposited palladium species cannot be washed out with excess acetone. On the other side, palladium can be leached out from the resulting materials by a treatment with aqueous solutions of acids or strongly complexing agents. For example, under the dispersion of the 2/ Al_2O_3 material in 2 M NaI (Figure S14) almost complete transfer of the Pd(II) into the solution occurs in the form of the $[\text{PdI}_4]^{2-}$ complex.⁶³ Analogously, complete desorption of Pd can be achieved with 2 M HNO_3 or 2 M HCl (but not with 2 M NaCl). These observations emphasize that Pd deposits from the solution of $(\text{R}_4\text{N})_2[\text{Pd}(\text{NO}_3)_4]$ salts as an ionic species and also support the proposed mechanism of Pd binding by surface $-\text{OH}$ groups. It is interesting to note in this context that oxide-supported palladium species can be easily reduced to metallic palladium by passing hydrogen through a suspension of the material (Figure S15).

To extend the range of the supporting materials, TiO_2 , SiO_2 , and $\text{Ni}(\text{OH})_2$ were also tested. $\text{Ni}(\text{OH})_2$ was introduced to probe the transition-metal hydroxide as a target support due to currently growing interest in bimetallic Pd-Ni materials for hydrogen energy applications: for example, in the oxygen reduction reaction⁶⁴ and catalytic decomposition of hydrazine hydrate (*vide infra*).^{65–67}

In all cases, with the exception of silica, fast palladium uptake was observed from an acetone solution of 2 (Figure 9A). Overall, the quantities of $[\text{Pd}(\text{NO}_3)_4]^{2-}$ that can be chemisorbed by a given oxide or hydroxide depend on the prehistory of this material (preparation method and conditions). For the materials used in this work, these values were estimated in experiments where the concentration of 2 was gradually increased, while the color of the supernatant was

controlled (see the Experimental Section). Up to 3 mol % of Pd can be deposited on Al_2O_3 and TiO_2 and 2 mol % can be sorbed by CeO_2 , while the uptake of $\text{Ni}(\text{OH})_2$ is up to 10 mol % of Pd. The inability of SiO_2 to interact with $[\text{Pd}(\text{NO}_3)_4]^{2-}$ anions can be explained by the lack of negatively charged $-\text{OH}$ groups on the surface with which to attack the palladium centers. On the other hand, this fact can be applied for the selective deposition of palladium on oxide or hydroxide materials dispersed over the SiO_2 matrix.

3.7. Catalytic Hydrogen Generation from Hydrazine Hydrate with $\text{Ni}_{0.9}\text{Pd}_{0.1}/\text{SiO}_2$. Previously, a synergetic effect was shown for Pd-Ni nanoparticles in the reaction of catalytic decomposition of hydrazine hydrate with the formation of H_2 .^{65,67} Hydrazine can decompose over metallic catalysts with (1) hydrogen formation, $\text{N}_2\text{H}_4 \rightarrow \text{N}_2 + 2\text{H}_2$, or (2) via a disproportionation reaction, $4\text{N}_2\text{H}_4 \rightarrow \text{N}_2 + 3\text{NH}_3$.⁶⁸ Both individual Ni and Pd nanoparticles show poor activity and selectivity, while the bimetallic nanoalloy $\text{Pd}_{40}\text{Ni}_{60}$ shows 80% H_2 selectivity (50 °C) with a relatively high rate of reaction.⁶⁵ Therefore, we examined the $[\text{Pd}(\text{NO}_3)_4]^{2-}$ chemisorption described above to prepare a Pd-Ni catalyst for the hydrazine hydrate decomposition process.

A silica-supported Pd-Ni catalyst was prepared by chemisorption of $[\text{Pd}(\text{NO}_3)_4]^{2-}$ species on SiO_2 -supported $\text{Ni}(\text{OH})_2$ particles from an acetone solution of 2. Treatment of the composite under a H_2 atmosphere at 400 °C results in the reduction of Pd and Ni to give the target $\text{Ni}_{0.9}\text{Pd}_{0.1}/\text{SiO}_2$ material containing 10 wt % of Ni and 2 wt % of Pd (as determined by X-ray fluorescence analysis). The XRD pattern of the as-prepared $\text{Ni}_{0.9}\text{Pd}_{0.1}/\text{SiO}_2$ catalyst shows highly intense and diffuse reflections of the SiO_2 matrix (Figure S16) as well as wide reflections attributed to small-sized metallic Pd particles. The positions of the reflections are slightly shifted in comparison to that of a Pd etalon, which can be attributed to the partial alloying with Ni.⁶⁷ Additionally, a broad line is observed at 61° corresponding to the NiO oxide phase that is well-known to cover highly dispersed Ni particles in an air atmosphere.^{69,70} The high-angle annular dark-field scanning TEM (HAADF-STEM) images and the corresponding elemental mappings demonstrate that in the $\text{Ni}_{0.9}\text{Pd}_{0.1}/\text{SiO}_2$

material Ni uniformly covers the surface of the SiO₂ support, while Pd particles, also being regularly distributed on the surface, are mainly concentrated in well-defined domains (Figure 10). These Pd-rich domains are observed in HR-TEM images (Figure S17) as particles with a size of about 5–7 nm with clearly defined interplanar distances of 2.2 Å attributed to the (111) facets of the face-centered cubic Pd.⁶⁴

The survey X-ray photoelectron spectrum of Ni_{0.9}Pd_{0.1}/SiO₂ has shown that silicon, oxygen, carbon, palladium, and nickel are situated on the surface. An analysis of the Pd 3d region reveals the presence of a single palladium form with a binding energy of 335.3 eV (Figure S18), which is typical for metallic Pd.⁷¹ In the Ni 2p_{3/2} range the only nickel species is observed with a binding energy of 856.5 eV, attributed to the surface NiO.⁷⁰ The Ni_{0.9}Pd_{0.1}/SiO₂ material was further tested in a hydrazine hydrate decomposition reaction.

At 50 °C, the Ni_{0.9}Pd_{0.1}/SiO₂ catalyst shows up to 80% H₂ selectivity with a TOF value of about 13 h⁻¹ per Pd atom. Experiments were also performed to test the stability of the Ni_{0.9}Pd_{0.1}/SiO₂ catalyst.⁶⁵ After each step, when N₂H₄ was depleted, a new portion of hydrazine hydrate was introduced. It can be clearly seen from Figure 11 that the catalyst shows

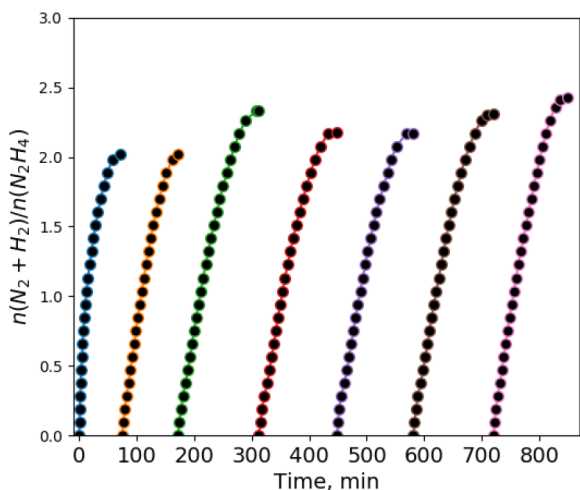


Figure 11. Durability experiments for H₂ generation from N₂H₄·H₂O using a Ni_{0.9}Pd_{0.1}/SiO₂ catalyst (300 mg) at 50 °C. C(NaOH) = 1 M, $n(\text{N}_2\text{H}_4)/n(\text{Pd}) = 16.3$.

stable hydrogen production over seven cycles, without notable deactivation. Interestingly, during the first step, the initial rate of the reaction is almost twice as high as the average rate on all of the next stages, while the selectivity grows slightly from cycle to cycle. This fact can be attributed to the gradual reduction of the oxide layer, covering the nickel surface (Figure S18), under the reductive reaction conditions. An examination of the spent Ni_{0.9}Pd_{0.1}/SiO₂ catalyst (after durability tests) with XRD (Figure S16) and HAADF-STEM and HR-TEM (Figure S19) does not show notable changes in the morphology of the catalyst in comparison to the as-prepared material. The intensities of reflections corresponding to metallic phases in the XRD pattern of the spent catalyst are slightly higher than in the case of the as-prepared material, which can be due to partial dissolution of the SiO₂ matrix in an alkaline media. These findings also agree well with the XPS results, which indicate that the nickel and palladium surface species remain unchanged (NiO and Pd⁰) under the reaction condition but

the M/Si (M = Ni, Pd) ratios increase considerably (Figure S18 and Table S7).

Among the catalysts tested so far for hydrazine decomposition, the supported M-Ni materials with M = Pt, Ir, Rh have shown superior rates of H₂ evolution (TOF values up to 400 h⁻¹) and almost 100% H₂ selectivity, while the palladium analogues demonstrated lower selectivity and TOF values.^{8,66} An analogous tendency is observed for cobalt-containing catalysts promoted with noble metals.⁷² At the same time, it should be noted that the preparation method and precursors highly influence the activity of the resulting catalysts; therefore, new preparation techniques for such materials are crucial for further development.⁷³ The parameters achieved in this work are close to the results reported earlier for Pd₃₀Ni₇₀ and Pd₄₀Ni₆₀ nanoparticles under the same conditions ($n(\text{N}_2\text{H}_4)/n(\text{catalyst}) = 10$),⁶⁵ which is quite an important achievement with regard to the reduction of the percentage of noble metals in catalysts.

4. CONCLUSIONS

In summary, the series of quaternary ammonium tetranitratopalladates (R₄N)₂[Pd(NO₃)₄] described here are non-hydroscopic and demonstrate high stability under normal conditions, in contrast to the commonly used palladium(II) nitrate. On the other hand, the given salts are highly soluble in various solvents, while the nitrate ligands can be readily substituted by an appropriate donor fragment. These properties, in combination with a high-yielding synthesis and thermostability (that is a general characteristic of transition-metal nitrate complexes), ensure their applicability as straightforward starting materials for the synthesis of palladium compounds and the preparation of Pd-containing catalysts.

In the current work, the aforementioned aspects were implemented by (a) the synthesis of compounds 4 and 5, starting from salt 2, and (b) the Pd deposition on various supports from solutions of (R₄N)₂[Pd(NO₃)₄] salts and the preparation of a Ni_{0.9}Pd_{0.1}/SiO₂ catalyst. To outline the other perspectives, it should be noted that palladium nitrate complexes can be utilized as homogeneous catalysts for alkene nitration,¹² as starting materials for the preparation of heterometallic compounds,⁷⁴ or in electrolytes for palladium electrodeposition.⁷⁵ It is also worth noting that nitrate complexes of palladium are components of spent nuclear fuel and their separation is crucial for the stability of the vitreous solid used for prolonged storage of high-level waste.⁷⁶ Therefore, in view of the noted wide range of applications, we believe that the tetranitratopalladates 1–3 will find their place in the arsenal of chemists.

■ ASSOCIATED CONTENT

Supporting Information

The Supporting Information is available free of charge at <https://pubs.acs.org/doi/10.1021/acs.inorgchem.0c03038>.

Additional crystallographic data, XRD data, NMR, IR, XPS, and MS spectra, additional micrographs, DFT-computed IR spectra, ELF plots, and relaxed PES scan data (PDF)

Accession Codes

CCDC 2008746, 2025660, 2026407, and 2026628 contain the supplementary crystallographic data for this paper. These data can be obtained free of charge via www.ccdc.cam.ac.uk/data_request/cif, or by emailing data_request@ccdc.cam.ac.

uk, or by contacting The Cambridge Crystallographic Data Centre, 12 Union Road, Cambridge CB2 1EZ, UK; fax: +44 1223 336033.

AUTHOR INFORMATION

Corresponding Author

Danila Vasilchenko – Nikolaev Institute of Inorganic Chemistry, Siberian Branch of the Russian Academy of Science, 630090 Novosibirsk, Russian Federation; orcid.org/0000-0002-4233-2105; Email: vasilchenko@niic.nsc.ru

Authors

Polina Topchiyan – Nikolaev Institute of Inorganic Chemistry, Siberian Branch of the Russian Academy of Science, 630090 Novosibirsk, Russian Federation; orcid.org/0000-0002-0827-4917

Semen Berdyugin – Nikolaev Institute of Inorganic Chemistry, Siberian Branch of the Russian Academy of Science, 630090 Novosibirsk, Russian Federation; orcid.org/0000-0003-3560-6873

Pavel Plyusnin – Nikolaev Institute of Inorganic Chemistry, Siberian Branch of the Russian Academy of Science, 630090 Novosibirsk, Russian Federation; orcid.org/0000-0002-7494-6240

Vladimir Shayapov – Nikolaev Institute of Inorganic Chemistry, Siberian Branch of the Russian Academy of Science, 630090 Novosibirsk, Russian Federation

Iraida Baidina – Nikolaev Institute of Inorganic Chemistry, Siberian Branch of the Russian Academy of Science, 630090 Novosibirsk, Russian Federation

Vladislav Komarov – Nikolaev Institute of Inorganic Chemistry, Siberian Branch of the Russian Academy of Science, 630090 Novosibirsk, Russian Federation

Andrey Bukhtiyarov – Boreskov Institute of Catalysis, 630090 Novosibirsk, Russia; orcid.org/0000-0002-0199-8111

Evgeny Gerasimov – Boreskov Institute of Catalysis, 630090 Novosibirsk, Russia

Complete contact information is available at:

<https://pubs.acs.org/10.1021/acs.inorgchem.0c03038>

Notes

The authors declare no competing financial interest.

ACKNOWLEDGMENTS

The authors deeply acknowledge S. V. Tkachev for the ^{15}N NMR data, Dr. A. P. Zubareva for assistance with the CHN analysis, Dr. B. A. Kolesov for the Raman spectroscopy data, and Dr. E. Yu. Filatov and Dr. Yu. V. Shubin for their assistance with XRPD. The authors thank the XRD Facility of NIIC SB RAS for the single-crystal data collection. The TEM and XPS experiments were performed using facilities of the shared research centre “National Center for the Investigation of Catalysts” at the Boreskov Institute of Catalysis.

REFERENCES

- (1) Cowley, A. *PGM Market Report, February 2020*; Johnson Matthey PLC. Retrieved from <http://www.platinum.matthey.com>, 2019.
- (2) Shelef, M.; McCabe, R. Twenty-Five Years after Introduction of Automotive Catalysts: What Next? *Catal. Today* **2000**, *62* (1), 35–50.
- (3) Slavinskaya, E. M.; Zadesenets, A. V.; Stonkus, O. A.; Stadnichenko, A. I.; Shchukarev, A. V.; Shubin, Y. V.; Korenev, S.

V.; Boronin, A. I. Thermal Activation of Pd/CeO₂-SnO₂ Catalysts for Low-Temperature CO Oxidation. *Appl. Catal., B* **2020**, *277* (March), 119275.

(4) Wang, Z.-Q.; Sun, J.; Xu, Z.-N.; Guo, G.-C. CO Direct Esterification to Dimethyl Oxalate and Dimethyl Carbonate: The Key Functional Motifs for Catalytic Selectivity. *Nanoscale* **2020**, *12*, 20131.

(5) Azarpour, A.; Zahedi, G. Performance Analysis of Crude Terephthalic Acid Hydrogenation in an Industrial Trickle-Bed Reactor Experiencing Catalyst Deactivation. *Chem. Eng. J.* **2012**, *209*, 180–193.

(6) Tourani, S.; Khorasheh, F.; Rashidi, A. M.; Safekordi, A. A. Hydro-Purification of Crude Terephthalic Acid Using Palladium Catalyst Supported on Multi-Wall Carbon Nanotubes. *J. Ind. Eng. Chem.* **2015**, *28*, 202–210.

(7) Banham, D.; Ye, S. Current Status and Future Development of Catalyst Materials and Catalyst Layers for Proton Exchange Membrane Fuel Cells: An Industrial Perspective. *ACS Energy Lett.* **2017**, *2* (3), 629–638.

(8) Cheng, Y.; Wu, X.; Xu, H. Catalytic Decomposition of Hydrous Hydrazine for Hydrogen Production. *Sustain. Energy Fuels* **2019**, *3* (2), 343–365.

(9) Dong, Y.; Chen, Q.; Qiu, C.; Ma, X.; Wang, Y.; Sun, T.; Fan, G. Synergistic Catalysis of Pd-Ni(OH)₂ Hybrid Anchored on Porous Carbon for Hydrogen Evolution from the Dehydrogenation of Formic Acid. *Int. J. Hydrogen Energy* **2020**, *45* (23), 12849–12858.

(10) Al-Azri, Z. H. N.; Chen, W.-T.; Chan, A.; Jovic, V.; Ina, T.; Idriss, H.; Waterhouse, G. I. N. The Roles of Metal Co-Catalysts and Reaction Media in Photocatalytic Hydrogen Production: Performance Evaluation of M/TiO₂ Photocatalysts (M = Pd, Pt, Au) in Different Alcohol-Water Mixtures. *J. Catal.* **2015**, *329*, 355–367.

(11) Yang, Y.; Chang, C.; Idriss, H. Photo-Catalytic Production of Hydrogen Form Ethanol over M/TiO₂ Catalysts (M = Pd, Pt or Rh). *Appl. Catal., B* **2006**, *67* (3–4), 217–222.

(12) Wenzel, T. T. Palladium(II) Nitrate. In *Encyclopedia of Reagents for Organic Synthesis*; Wiley: Chichester, U.K., 2001; p 1. DOI: 10.1002/047084289X.rp013.

(13) Laligant, Y.; Ferey, G.; Le Bail, A. Crystal Structure of Pd(NO₃)₂(H₂O)₂. *Mater. Res. Bull.* **1991**, *26* (4), 269–275.

(14) Khramenko, S. P.; Baidina, I. A.; Gromilov, S. A. Crystal Structure Refinement for Trans-[Pd(NO₃)₂(H₂O)₂]. *J. Struct. Chem.* **2007**, *48* (6), 1152–1155.

(15) Venediktov, A. B.; Korenev, S. V.; Khramenko, S. P.; Tkachev, S. V.; Plyusnin, P. E.; Mamonov, S. N.; Ivanova, L. V.; Vostrikov, V. a. Properties of Nitric Acid Palladium Solutions with a High Metal Concentration. *Russ. J. Appl. Chem.* **2007**, *80* (5), 695–704.

(16) Vasilchenko, D. B.; Gulyaev, R. V.; Slavinskaya, E. M.; Stonkus, O. A.; Shubin, Y. V.; Korenev, S. V.; Boronin, A. I. Effect of Pd Deposition Procedure on Activity of Pd/Ce_{0.5}Sn_{0.5}O₂ Catalysts for Low-Temperature CO Oxidation. *Catal. Commun.* **2016**, *73*, 34–38.

(17) Inci, D.; Aydin, R.; Vatan, Ö.; Şahin, O.; Çinkiliç, N. Water-Soluble Binary and Ternary Palladium(II) Complexes Containing Amino Acids and Intercalating Ligands: Synthesis, Characterization, Biomolecular Interactions and Cytotoxicities. *New J. Chem.* **2019**, *43* (12), 4681–4697.

(18) Wickleder, M. S.; Gerlach, F.; Gagelmann, S.; Bruns, J.; Fenske, M.; Al-Shamery, K. Thermolabile Noble Metal Precursors: (NO)-[Au(NO₃)₄], (NO)₂[Pd(NO₃)₄], and (NO)₂[Pt(NO₃)₆]. *Angew. Chem., Int. Ed.* **2012**, *51* (9), 2199–2203.

(19) Bruns, J.; Klüner, T.; Wickleder, M. S. Oxoanionic Noble Metal Compounds from Fuming Nitric Acid: The Palladium Examples Pd(NO₃)₂ and Pd(CH₃SO₃)₂. *Chem. - Eur. J.* **2015**, *21* (3), 1294–1301.

(20) Khramenko, S. P.; Baidina, I. A.; Gromilov, S. A.; Belyaev, A. V. Synthesis and X-Ray Investigation of Rb₂[Pd(NO₃)₄] and Cs₂[Pd(NO₃)₄]. *J. Struct. Chem.* **2005**, *46* (6), 1060–1065.

(21) Khramenko, S. P.; Baidina, I. A.; Kuratieva, N. V.; Gromilov, S. A. X-Ray Structure of KCs[Pd(NO₃)₄]-0.5H₂O. *J. Struct. Chem.* **2009**, *50* (1), 166–169.

- (22) Khranenko, S. P.; Baidina, I. A.; Gromilov, S. A. Crystal Structure of a New Polymorphic Modification of β -K₂[Pd(NO₃)₄]. *J. Struct. Chem.* **2009**, *50* (2), 361–364.
- (23) Vasilchenko, D.; Topchiyan, P.; Berdyugin, S.; Filatov, E.; Tkachev, S.; Baidina, I.; Komarov, V.; Slavinskaya, E.; Stadnichenko, A.; Gerasimov, E. Tetraalkylammonium Salts of Platinum Nitrate Complexes: Isolation, Structure, and Relevance to the Preparation of PtO_x/CeO₂ Catalysts for Low-Temperature CO Oxidation. *Inorg. Chem.* **2019**, *58* (9), 6075–6087.
- (24) Vasilchenko, D.; Tkachev, S.; Baidina, I.; Korenev, S. Speciation of Platinum(IV) in Nitric Acid Solutions. *Inorg. Chem.* **2013**, *52* (18), 10532–10541.
- (25) Vasilchenko, D.; Asanova, T.; Kolesov, B.; Tsygankova, A.; Stadnichenko, A.; Slavinskaya, E.; Gerasimov, E.; Lomachenko, K.; Boronin, A.; Korenev, S. Cerium(III) Nitrate Derived CeO₂ Support Stabilising PtO_x Active Species for Room Temperature CO Oxidation. *ChemCatChem* **2020**, *12* (5), 1413–1428.
- (26) Vasilchenko, D.; Topchiyan, P.; Tsygankova, A.; Asanova, T.; Kolesov, B.; Bukhtiyarov, A.; Kurenkova, A.; Kozlova, E. Photo-induced Deposition of Platinum from (Bu₄N)₂[Pt(NO₃)₆] for a Low Pt-Loading Pt/TiO₂ Hydrogen Photogeneration Catalyst. *ACS Appl. Mater. Interfaces* **2020**, *12* (43), 48631–48641.
- (27) Shipsey, K.; Werner, E. A. CXXXII.—The Purification of Acetone by Means of Sodium Iodide. *J. Chem. Soc., Trans.* **1913**, 103 (c), 1255–1257.
- (28) Calderazzo, F.; Marchetti, F.; Pampaloni, G.; Passarelli, V. Coordination Properties of 1,10-Phenanthroline-5,6-Dione towards Group 4 and 5 Metals in Low and High Oxidation States †. *J. Chem. Soc., Dalton Trans.* **1999**, No. 24, 4389–4396.
- (29) Scofield, J. H. Hartree-Slater Subshell Photoionization Cross-Sections at 1254 and 1487 eV. *J. Electron Spectrosc. Relat. Phenom.* **1976**, *8* (2), 129–137.
- (30) Sheldrick, G. M. Crystal Structure Refinement with SHELXL. *Acta Crystallogr., Sect. C: Struct. Chem.* **2015**, *71* (1), 3–8.
- (31) SADABS; Bruker AXS Inc.: Madison, WI, USA, 2001.
- (32) Spackman, M. A.; Jayatilaka, D. Hirshfeld Surface Analysis. *CrystEngComm* **2009**, *11* (1), 19–32.
- (33) Frisch, M. J.; Trucks, G. W.; Schlegel, H. B.; Scuseria, G. E.; Robb, M. A.; Cheeseman, J. R.; Scalmani, G.; Barone, V.; Petersson, G. A.; Nakatsuji, H.; Li, X.; Caricato, M.; Marenich, A.; Bloino, J.; Janesko, B. G.; Gomperts, R.; Mennucci, B.; Hratchian, H. P.; Ortiz, J. V.; Izmaylov, A. F.; Sonnenberg, J. L.; Williams-Young, D.; Ding, F.; Lipparini, F.; Egidi, F.; Goings, J.; Peng, B.; Petrone, A.; Henderson, T.; Ranasinghe, D.; Zakrzewski, V. G.; Gao, J.; Rega, N.; Zheng, G.; Liang, W.; Hada, M.; Ehara, M.; Toyota, K.; Fukuda, R.; Hasegawa, J.; Ishida, M.; Nakajima, T.; Honda, Y.; Kitao, O.; Nakai, H.; Vreven, T.; Throssell, K.; Montgomery, J. A., Jr.; Peralta, J. E.; Ogliaro, F.; Bearpark, M.; Heyd, J. J.; Brothers, E.; Kudin, K. N.; Staroverov, V. N.; Keith, T.; Kobayashi, R.; Normand, J.; Raghavachari, K.; Rendell, A.; Burant, J. C.; Iyengar, S. S.; Tomasi, J.; Cossi, M.; Millam, J. M.; Klene, M.; Adamo, C.; Cammi, R.; Ochterski, J. W.; Martin, R. L.; Morokuma, K.; Farkas, O.; Foresman, J. B.; Fox, D. J. *Gaussian 09, Rev. C*; Gaussian, Inc.: Wallingford, CT, 2009.
- (34) Vosko, S. H.; Wilk, L.; Nusair, M. Accurate Spin-Dependent Electron Liquid Correlation Energies for Local Spin Density Calculations: A Critical Analysis. *Can. J. Phys.* **1980**, *58* (8), 1200–1211.
- (35) Lee, C.; Yang, W.; Parr, R. G. Development of the Colle-Salvetti Correlation-Energy Formula into a Functional of the Electron Density. *Phys. Rev. B: Condens. Matter Mater. Phys.* **1988**, *37* (2), 785–789.
- (36) Becke, A. D. Density-functional Thermochemistry. III. The Role of Exact Exchange. *J. Chem. Phys.* **1993**, *98* (7), 5648–5652.
- (37) Stephens, P. J.; Devlin, F. J.; Chabalowski, C. F.; Frisch, M. J. Ab Initio Calculation of Vibrational Absorption and Circular Dichroism Spectra Using Density Functional Force Fields. *J. Phys. Chem.* **1994**, *98* (45), 11623–11627.
- (38) Hehre, W. J.; Stewart, R. F.; Pople, J. A. Self-Consistent Molecular-Orbital Methods. I. Use of Gaussian Expansions of Slater-Type Atomic Orbitals. *J. Chem. Phys.* **1969**, *51* (6), 2657–2664.
- (39) Hay, P. J.; Wadt, W. R. Ab Initio Effective Core Potentials for Molecular Calculations. Potentials for K to Au Including the Outermost Core Orbitals. *J. Chem. Phys.* **1985**, *82* (1), 299–310.
- (40) Collins, J. B.; Schleyer, P. v. R.; Binkley, J. S.; Pople, J. A. Self-consistent Molecular Orbital Methods. XVII. Geometries and Binding Energies of Second-row Molecules. A Comparison of Three Basis Sets. *J. Chem. Phys.* **1976**, *64* (12), S142–S151.
- (41) Wadt, W. R.; Hay, P. J. Ab Initio Effective Core Potentials for Molecular Calculations. Potentials for Main Group Elements Na to Bi. *J. Chem. Phys.* **1985**, *82* (1), 284–298.
- (42) Hay, P. J.; Wadt, W. R. Ab Initio Effective Core Potentials for Molecular Calculations. Potentials for the Transition Metal Atoms Sc to Hg. *J. Chem. Phys.* **1985**, *82* (1), 270–283.
- (43) Tomasi, J.; Mennucci, B.; Cammi, R. Quantum Mechanical Continuum Solvation Models. *Chem. Rev.* **2005**, *105* (8), 2999–3094.
- (44) Baerends, E. J.; Ziegler, T.; Atkins, A. J.; Autschbach, J.; Bashford, D.; Baseggio, O.; Bérces, A.; Bickelhaupt, F. M.; Bo, C.; Boerrigter, P. M.; Cavallo, L.; Daul, C.; Chong, D. P.; Chulhai, D. V.; Deng, L.; Dickson, R. M.; Dieterich, J. M.; Ellis, D. E.; van Faassen, M.; Ghysels, A.; Giammona, A.; van Gisbergen, S. J. A.; Goetz, A.; Götz, A. W.; Gusarov, S.; Harris, F. E.; van den Hoek, P.; Hu, Z.; Jacob, C. R.; Jacobsen, H.; Jensen, L.; Joubert, L.; Kaminski, J. W.; van Kessel, G.; König, C.; Kootstra, F.; Kovalenko, A.; Krykunov, M.; van Lenthe, E.; McCormack, D. A.; Michalak, A.; Mitoraj, M.; Morton, S. M.; Neugebauer, J.; Nicu, V. P.; Noodleman, L.; Osinga, V. P.; Patchkovskii, S.; Pavanello, M.; Peeples, C. A.; Philipsen, P. H. T.; Post, D.; Pye, C. C.; Ramanantoanina, H.; Ramos, P.; Ravenek, W.; Rodriguez, J. I.; Ros, P.; Rüger, R.; Schipper, P. R. T.; Schlüß, D.; van Schoot, H.; Schreckenbach, G.; Seldenthuis, J. S.; Seth, M.; Snijders, J. G.; Solà, M.; M, S.; Swart, M.; Swerhone, D.; te Velde, G.; Tognetti, V.; Vernooijs, P.; Versluis, L.; Visscher, L.; Visser, O.; Wang, F.; Wesolowski, T. A.; van Wezenbeek, E. M.; Wiesenekker, G.; Wolff, S. K.; Woo, T. K.; Yakovlev, A. L. *ADF2016*; SCM, Theoretical Chemistry, Vrije Universiteit: Amsterdam, The Netherlands, 2016; <https://www.scm.com>.
- (45) Klamt, A.; Schüürmann, G. COSMO: A New Approach to Dielectric Screening in Solvents with Explicit Expressions for the Screening Energy and Its Gradient. *J. Chem. Soc., Perkin Trans. 2* **1993**, No. 5, 799–805.
- (46) Frias, E. Palladium Complexes in Concentrated Nitrate and Acid Solutions. *Talanta* **1995**, *42* (11), 1675–1683.
- (47) Vasilchenko, D. B.; Tkachev, S. V.; Tsipis, A. C. Aquanitrato Complexes of Palladium, Rhodium, and Platinum: A Comparative 15 N NMR and DFT Study. *Eur. J. Inorg. Chem.* **2018**, *2018* (5), 627–639.
- (48) Purans, J.; Fourest, B.; Cannes, C.; Sladkov, V.; David, F.; Venault, L.; Lecomte, M. Structural Investigation of Pd(II) in Concentrated Nitric and Perchloric Acid Solutions by XAFS. *J. Phys. Chem. B* **2005**, *109* (21), 11074–11082.
- (49) Nakamoto, K. *Infrared and Raman Spectra of Inorganic and Coordination Compounds, Part B*, 6th ed.; Wiley: 2009.
- (50) Addison, C. C.; Sutton, D. Complexes Containing the Nitrate Ion. In *Progress in Inorganic Chemistry* **2007**, *8*, 195–286.
- (51) Addison, C. C.; Brownlee, G. S.; Logan, N. Tetranitratoaurates-(III): Preparation, Spectra, and Properties. *J. Chem. Soc., Dalton Trans.* **1972**, No. 14, 1440.
- (52) Vasilchenko, D.; Vorobieva, S.; Baidina, I.; Piryazev, D.; Tsipis, A.; Korenev, S. Structure and Properties of a Rhodium(III) Pentanitrato Complex Embracing Uni- and Bidentate Nitrate Ligands. *Polyhedron* **2018**, *147*, 69–74.
- (53) Fujii, T.; Egusa, S.; Uehara, A.; Kirishima, A.; Yamagishi, I.; Morita, Y.; Yamana, H. Electronic Absorption Spectra of Palladium-(II) in Concentrated Nitric Acid Solutions. *J. Radioanal. Nucl. Chem.* **2011**, *290* (2), 475–478.

- (54) Jørgensen, C. K.; Parthasarathy, V.; Ahlgrén, M.; Rantala, M. The Influence of Nitrate and Other Anions on the Absorption Spectra of Palladium(II). *Acta Chem. Scand.* **1978**, *32a*, 957–962.
- (55) Bastian, R.; Weberling, R.; Palilla, F. Ultraviolet Spectrophotometric Determination of Nitrate—Application to Analysis of Alkaline Carbonates. *Anal. Chem.* **1957**, *29* (12), 1795–1797.
- (56) Addison, C. C.; Logan, N.; Wallwork, S. C.; Garner, C. D. Structural Aspects of Co-Ordinated Nitrate Groups. *Q. Rev., Chem. Soc.* **1971**, *25* (2), 289.
- (57) Khramenko, S. P.; Baidina, I. A.; Gromilov, S. A.; Belyaev, A. V. Synthesis and Crystal Structure of Na₂[Pd(NO₃)₄]. *J. Struct. Chem.* **2000**, *41* (4), 709–712.
- (58) Sun, C.-F.; Hu, C.-L.; Xu, X.; Mao, J.-G. Polar or Non-Polar? Syntheses, Crystal Structures, and Optical Properties of Three New Palladium(II) Iodates. *Inorg. Chem.* **2010**, *49* (20), 9581–9589.
- (59) Rasmussen, L.; Jørgensen, C. K. Palladium(II) Complexes. I. Spectra and Formation Constants of Ammonia and Ethylenediamine Complexes. *Acta Chem. Scand.* **1968**, *22*, 2313–2323.
- (60) Pilný, R.; Lubal, P.; Elding, L. I. Thermodynamics for Complex Formation between Palladium(II) and Oxalate. *Dalt. Trans.* **2014**, *43* (32), 12243–12250.
- (61) Calderazzo, F.; Pampaloni, G.; Passarelli, V. 1,10-Phenanthroline-5,6-Dione as a Building Block for the Synthesis of Homo- and Heterometallic Complexes. *Inorg. Chim. Acta* **2002**, *330* (1), 136–142.
- (62) Parac, T. N.; Kostić, N. M. New Selectivity and Turnover in Peptide Hydrolysis by Metal Complexes. A Palladium(II) Aqua Complex Catalyzes Cleavage of Peptides Next to the Histidine Residue. *J. Am. Chem. Soc.* **1996**, *118* (1), 51–58.
- (63) Yamamoto, K.; Fujibayashi, T.; Motomizu, S. Liquid-Liquid Distribution of Ion Associates of Tetrahalogenopalladate(II) with Quaternary Ammonium Counter Ions. *Solvent Extr. Ion Exch.* **1992**, *10* (3), 459–476.
- (64) Feng, Y.; Shao, Q.; Ji, Y.; Cui, X.; Li, Y.; Zhu, X.; Huang, X. Surface-Modulated Palladium-Nickel Icosahedra as High-Performance Non-Platinum Oxygen Reduction Electrocatalysts. *Sci. Adv.* **2018**, *4* (7), No. eaap8817.
- (65) Singh, S. K.; Iizuka, Y.; Xu, Q. Nickel-Palladium Nanoparticle Catalyzed Hydrogen Generation from Hydrous Hydrazine for Chemical Hydrogen Storage. *Int. J. Hydrogen Energy* **2011**, *36* (18), 11794–11801.
- (66) Song, X.; Yang, P.; Wang, J.; Zhao, X.; Zhou, Y.; Li, Y.; Yang, L. NiFePd/UiO-66 Nanocomposites as Highly Efficient Catalysts to Accelerate Hydrogen Evolution from Hydrous Hydrazine. *Inorg. Chem. Front.* **2019**, *6* (10), 2727–2735.
- (67) Bhattacharjee, D.; Mandal, K.; Dasgupta, S. High Performance Nickel and Palladium Nanocatalyst for Hydrogen Generation from Alkaline Hydrous Hydrazine at Room Temperature. *J. Power Sources* **2015**, *287*, 96–99.
- (68) Singh, S. K.; Zhang, X.-B.; Xu, Q. Room-Temperature Hydrogen Generation from Hydrous Hydrazine for Chemical Hydrogen Storage. *J. Am. Chem. Soc.* **2009**, *131* (29), 9894–9895.
- (69) Zhang, K.; Mukhriza, T.; Liu, X.; Greco, P. P.; Chiremba, E. A Study on CO₂ and CH₄ Conversion to Synthesis Gas and Higher Hydrocarbons by the Combination of Catalysts and Dielectric-Barrier Discharges. *Appl. Catal., A* **2015**, *502* (4), 138–149.
- (70) Liu, Y.; Sheng, W.; Hou, Z.; Zhang, Y. Homogeneous and Highly Dispersed Ni-Ru on a Silica Support as an Effective CO Methanation Catalyst. *RSC Adv.* **2018**, *8* (4), 2123–2131.
- (71) Khudorozhkov, A. K.; Chetyrin, I. A.; Bukhtiyarov, A. V.; Prosvirin, I. P.; Bukhtiyarov, V. I. Propane Oxidation Over Pd/Al₂O₃: Kinetic and In Situ XPS Study. *Top. Catal.* **2017**, *60* (1–2), 190–197.
- (72) Firdous, N.; Janjua, N. K.; Wattoo, M. H. S. Promoting Effect of Ruthenium, Platinum and Palladium on Alumina Supported Cobalt Catalysts for Ultimate Generation of Hydrogen from Hydrazine. *Int. J. Hydrogen Energy* **2020**, *45* (41), 21573–21587.
- (73) Singh, S. K.; Xu, Q. Nanocatalysts for Hydrogen Generation from Hydrazine. *Catal. Sci. Technol.* **2013**, *3* (8), 1889.
- (74) Komarek, A. C.; Merz, P.; Guo, H.; Suard, E.; Chen, J.-M.; Felser, C.; Jansen, M. Pb₂PdO₂(OH)₂ and Pb₂PdO(OH)₄(H₂O): Synthesis and Crystal Growth at Ambient Conditions. *Z. Anorg. Allg. Chem.* **2015**, *641* (8–9), 1473–1479.
- (75) Liu, S.; Liu, R.; Wu, Y.; Wei, Y.; Fang, B. Study on Electrochemical Properties of Palladium in Nitric Acid Medium. *Energy Procedia* **2013**, *39*, 387–395.
- (76) Kolarik, Z.; Renard, E. Recovery of Value Fission Platinoids from Spent Nuclear Fuel. *Platin. Met. Rev.* **2003**, No. 2, 74–87.